ChemPubSoc Europe

DOI: 10.1002/chem.201304626

CHEMISTRY A European Journal Full Paper

Diazaporphyrins

Covalently Linked 5,15-Diazaporphyrin Dimers: Promising Scaffolds for a Highly Conjugated Azaporphyrin π System

Yoshihiro Matano,*[a] Daisuke Fujii,[b] Tarou Shibano,[b] Ko Furukawa,[c] Tomohiro Higashino,[b] Haruyuki Nakano,[d] and Hiroshi Imahori*[b, e]

Abstract: The first examples of β–β directly linked, acetylene-bridged, and butadiyne-bridged 5,15-diazaporphyrin dimers have been prepared by palladium-catalyzed coupling reactions of nickel(II) and copper(II) complexes of 3-bromo-10,20-dimesityl-5,15-diazaporphyrin (mesityl = 2,4,6-trimethylphenyl). The effects of the linking modes and *meso*-nitrogen atoms on the structural, optical, electrochemical, and magnetic properties of the distributed π systems were investigated by using X-ray crystallography, UV/Vis absorption spectroscopy, DFT calculations, cyclic voltammetry, and ESR spectroscopy. Both the electronic and steric effects of the *meso*-nitrogen atoms play an important role in the highly coplanar geometry of the directly linked dimers. The direct β–β linkage produces enhanced π conjugation and electron-spin coupling between the two diazaporphyrin units.

Introduction

Recent advances in porphyrin-based materials chemistry have highlighted covalently linked porphyrin dimers (diporphyrins) as potential nonlinear optical materials, singlet oxygen sensitizers, and imaging agents.[1] One key aspect is the rationalization of linker effects on the electronic and magnetic communications between two metalloporphyrin units, as this provides valuable information on the molecular design of new porphyrin-based functional materials. It is well known that the orientation and degree of π conjugation between the two porphyrins are strongly dependent on the linking modes. For example, acetylene-[2] and butadiyne-bridged[3] diporphyrins are highly conjugated, whereas β–β- and *meso*–*meso*-directly linked diporphyrins are weakly conjugated owing to their twisted structures.[4] Osuka and co-workers established an efficient method to convert the *meso*–*meso* singly bonded, twisted diporphyrins to triply fused, coplanar diporphyrins,[5] which showed the characteristic properties of an extended π system.

5,15-Diazaporphyrin (DAP) possesses an intrinsic D_{2h}-symmetric π system with nondegenerate HOMOs and LUMOs. Owing to these orbital characteristics, the light-harvesting and electron-donating/-accepting abilities of DAPs differ considerably from those of porphyrins.[6] For example, DAPs exhibit red-shifted and more intense Q bands. To our knowledge, however, there have been no reports of covalently linked DAP dimers (bis-DAPs), and the effects of the linking mode and *meso*-nitrogen atoms on the structures and fundamental properties in a series of bis-DAPs have yet to be elucidated. Recently, we established convenient methods for the synthesis and peripheral functionalization of β-unsubstituted DAP–metal complexes.[7,8] The phenyl groups attached to the pyrrolic β-carbon atoms have proven capable of extending the conjugation of the DAP π system. Thus, β–β covalently linked bis-DAPs would be a promising design for highly conjugated azaporphyrin π systems. Herein, we report the first examples of β–β directly linked, acetylene-bridged, and butadiyne-bridged bis-DAPs with coordinated nickel(II) or copper(II). The structures and the electronic and magnetic properties of these newly prepared bis-DAPs will be discussed relative to those of the β–β-linked diporphyrin analogues.

Results and Discussion

Scheme 1 illustrates the synthesis of directly linked bis-NiDAP (**3 Ni**) and bis-CuDAP (**3 Cu**). Treatment of NiDAP[7] (**1 Ni**) with *N*-bromosuccinimide (NBS; 1 equiv) afforded 3-brominated NiDAP (**2 Ni**) as the major product. The palladium-catalyzed reductive homocoupling of **2 Ni** proceeded smoothly in the pres-

[a] *Prof. Dr. Y. Matano*
Department of Chemistry, Faculty of Science
Niigata University, Niigata 950-2181 (Japan)
E-mail: matano@chem.sc.niigata-u.ac.jp

[b] *D. Fujii, T. Shibano, T. Higashino, Prof. Dr. H. Imahori*
Department of Molecular Engineering
Graduate School of Engineering, Kyoto University
Nishikyo-ku, Kyoto 615-8510 (Japan)

[c] *Prof. Dr. K. Furukawa*
Center for Instrumental Analysis
Institute for Research Promotion, Niigata University
Nishi-ku, Niigata 950-2181 (Japan)

[d] *Prof. Dr. H. Nakano*
Department of Chemistry, Graduate School of Sciences
Kyushu University, Fukuoka 812-8581 (Japan)

[e] *Prof. Dr. H. Imahori*
Institute for Integrated Cell-Material Sciences (WPI-iCeMS)
Kyoto University, Nishikyo-ku, Kyoto 615-8510 (Japan)
E-mail: imahori@scl.kyoto-u.ac.jp

Supporting information for this article is available on the WWW under http://dx.doi.org/10.1002/chem.201304626.

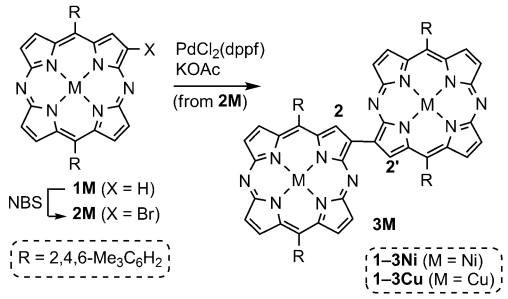

Scheme 1. Synthesis of **3 M** (M = Ni, Cu).

ence of KOAc to give **3 Ni** as a green solid. A similar protocol was employed in the synthesis of **3 Cu**, which was obtained from CuDAP[7a] (**1 Cu**) (Scheme 1).

Scheme 2 summarizes the synthesis of the acetylene- and butadiyne-bridged bis-NiDAPs. Sonogashira coupling of **2 Ni** with triisopropylsilylacetylene gave 3-(triisopropylsilylethynyl)-NiDAP (**4**), which was then converted to 3-(ethynyl)NiDAP (**5**)

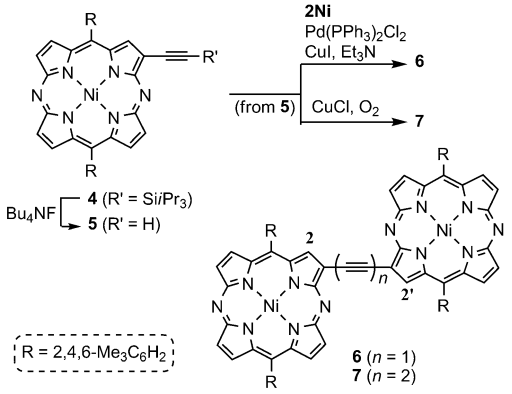

Scheme 2. Synthesis of **6** and **7**.

by treatment with tetrabutylammonium fluoride (Bu_4NF). Sonogashira coupling between **2 Ni** and **5** afforded acetylene-bridged bis-NiDAP (**6**). In addition, the copper-promoted oxidative homocoupling of **5** under dioxygen atmosphere afforded butadiyne-bridged bis-NiDAP (**7**) as the major product.

Compounds **3 Ni**, **3 Cu**, **6**, and **7** are the first reported examples of covalently linked bis-DAPs and have been characterized by ^{1}H NMR spectroscopy and high-resolution mass spectrometry. In the ^{1}H NMR spectra of **3 Ni**, **6**, and **7** in CD_2Cl_2, the pyrrolic β protons bound to the 2(2′)-carbon atoms (β-C^2–H) are observed at $\delta = 11.00$ ppm for **3 Ni**, $\delta = 9.25$ ppm for **6**, and $\delta = 8.95$ ppm for **7** as singlet peaks (Figure S1 in the Supporting Information). Notably, the β-C^2–H of **3 Ni** is strongly deshielded relative to **1 Ni** ($\delta = 8.78$ ppm; Figure 1). In addition, the downfield shift of the β-C^2–H of **3 Ni** ($\Delta\delta = 2.22$ ppm versus **1 Ni**) is considerably larger than those in **6** ($\Delta\delta = 0.47$ ppm) and **7** ($\Delta\delta = 0.17$ ppm). The β-C^2–H of Osuka's diporphyrin **8 H_2**[4h] (Scheme 3, $\delta = 9.76$ ppm) is less deshielded than **3 Ni**. These results indicate that the two *meso*-nitrogen (N^5) atoms play a crucial role in producing large deshielding effects on β-C^2–H in the directly linked bis-NiDAP **3 Ni** (see below).

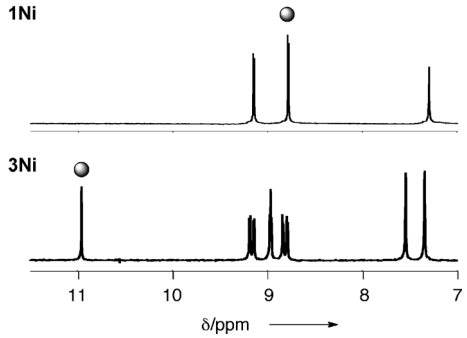

Figure 1. ^{1}H NMR spectra ($\delta = 7.0$–11.5 ppm) of **1 Ni** and **3 Ni** in CD_2Cl_2. Circles indicate the β proton at the 2(2′)-position.

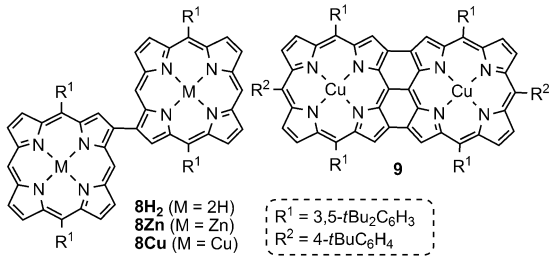

Scheme 3. Structures of Osuka's diporphyrins **8** and **9**.

The crystal structures of **3 Ni** and **3 Cu** were unambiguously elucidated by X-ray crystallography (Figure 2).[9] Each unit cell consists of two crystallographically independent molecules, which have similar structural parameters (Table S1 and Figure S2 in the Supporting Information). As shown in Figure 2a, the two DAP rings of **3 Ni** are almost in the same plane with a *trans* conformation (Ni···Ni = 9.7 Å).[9] The distance between the *meso*-N^5 and β-C^2–H atoms (ca. 2.5 Å) is shorter than the sum of their van der Waals radii (2.75 Å), thus implying that there is a hydrogen-bonding interaction between these two atoms.[10,11] It should be noted that the β–β directly linked diporphyrins adopt a far more twisted conformation.[12] Clearly, the unsubstituted and electronegative *meso*-nitrogen atoms play an important role in the coplanarization of the two DAP π systems, both sterically and electronically. The fact that the inter-ring C–C bond between the two DAP rings (1.449(3)–1.455(3) Å) is appreciably shorter than that between the DAP ring and the mesityl group (1.501(2)–1.508(2) Å) indicates the effective π conjugation between the two DAP units. The crystal structure of **3 Cu** (Cu···Cu = 9.8 Å) closely resembles that of **3 Ni** (Figure 2b).

To obtain further insight into the effects of the linkage on the structures of bis-DAPs, we conducted density functional theory (DFT) calculations at the B3LYP/6-311G(d,p) level on two models, **3 Ni-m** and **6-m**, in which the mesityl groups were replaced by hydrogen atoms (for details, see the Supporting Information). In the optimized structures, the two DAP rings were almost on the same plane with torsion angles (θ) about the inter-ring bonds of 177° for **3 Ni-m** and 180° for **6-m**

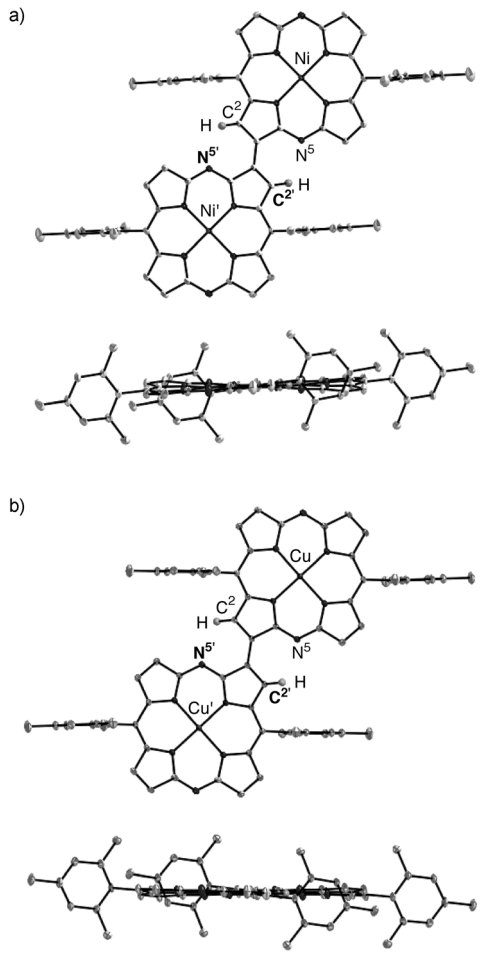

Figure 2. Crystal structures of a) **3Ni** and b) **3Cu** (one of the independent molecules; 30% probability ellipsoids): top view (upper) and side view (lower). Hydrogen atoms except for C^2–H are omitted for clarity.

(Figure 3). Over the range $0 \leq \theta \leq 30°$, the twisted conformation of **3Ni-m** is largely destabilized relative to the *trans* form ($\Delta E \geq 13$ kcal mol^{-1}), probably owing to the steric repulsion between the two DAP rings. In marked contrast, rotation-energy barriers of the acetylene-bridged dimer **6-m** are very small ($\Delta E < 2$ kcal mol^{-1}) over the range 0 to 180°. Both the experimental (X-ray) and theoretical (DFT) results strongly support the ^{1}H NMR spectroscopic observations: the large downfield

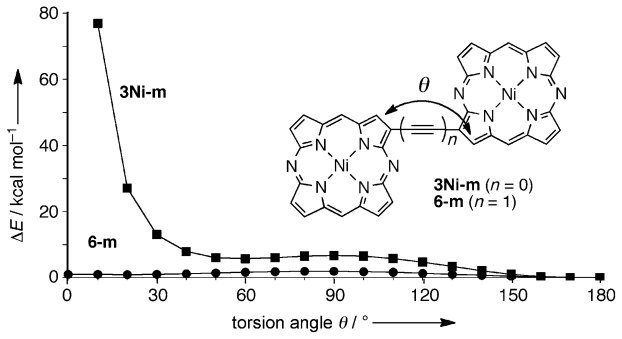

Figure 3. Potential energies (ΔE) of **3Ni-m** and **6-m** relative to *trans* conformers ($\theta = 180°$).

shift of the β-C^2–H of **3Ni** is attributable to a large ring-current effect from the adjacent DAP rings as well as the hydrogen-bonding interaction with the neighboring *meso*-N atom.

To investigate the optical properties of bis-DAPs, UV/Vis absorption spectra of **3M**, **6**, and **7** were measured in CH_2Cl_2 (Figure 4, Figure S4 in the Supporting Information, and Table 1). Both Soret and Q bands of **3M**, **6**, and **7** are broadened and redshifted relative to those of **1M**. The redshifts of

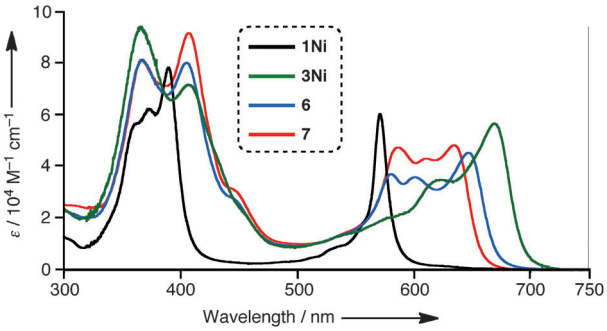

Figure 4. UV/Vis absorption spectra of **1Ni**, **3Ni**, **6**, and **7** in CH_2Cl_2.

the Q bands for **3M** ($\Delta\lambda_Q = 89$–98 nm versus **1M**) are significantly larger than that observed for the analogous diporphyrin **8Zn**[4k] (Scheme 3; $\lambda_Q = 586$ nm in toluene, $\Delta\lambda_Q = 11$ nm versus monomer[13]). In addition, the $\Delta\lambda_Q$ values increase in the order **7** (62 nm) < **6** (76 nm) < **3Ni** (98 nm) with the directly linked bis-NiDAP **3Ni** showing the most redshifted Q band. This indicates that **3Ni** has the narrowest HOMO–LUMO gap. The long-range time-correlated DFT calculations on **3Ni-m** and **6-m** also qualitatively support the observed difference in λ_Q values between **3Ni** and **6** (Figure S3 and Table S3 in the Supporting Information).

To assess the linkage effects on the electrochemical properties of the bis-DAPs, the redox potentials of **3M**, **6**, and **7** were measured in CH_2Cl_2 by using cyclic voltammetry (CV) and differential pulse voltammetry (DPV) with Bu_4NPF_6 as a supporting electrolyte (Table 1 and Figure S5 in the Supporting Information). As reported previously, **1Ni** showed a reversible oxidation process at +0.80 V (1 e$^-$) and reduction processes at −1.40 (1 e$^-$) and −2.02 V (1 e$^-$) within the observable range from −2.1 to +1.1 V (potentials versus ferrocene/ferrocenium (Fc/Fc^+)).[7] However, **3Ni** displayed reversible peaks at +0.74 (1 e$^-$) and +0.93 V (1 e$^-$) for the oxidation processes and at −1.18 (1 e$^-$), −1.37 (1 e$^-$), and −1.90 V (1 e$^-$) for the reduction processes. Similarly, **3Cu**, **6**, and **7** showed split peaks for the oxidation processes. The splitting of the redox processes is most likely due to electronic coupling of the two DAP π systems through the inter-ring covalent bonds. It should also be noted that the coupling energy observed for the oxidation processes of **3Ni** ($\Delta E_{ox} = 0.19$ V, $\Delta E_{ox} = E_{ox,2} - E_{ox,1}$) is larger than those of **6** ($E_{ox} = 0.14$ V) and **7** ($E_{ox} = 0.09$ V). Clearly, the direct linkage is more effective than the acetylene and butadiyne bridges in delocalizing the π electrons over the two DAP units. The electrochemical HOMO–LUMO gaps ($E_{ox,1} - E_{red,1}$) increase in the order **3Ni** (1.92 V) < **6** (2.05 V) < **7** (2.19 V), which agrees

Table 1. Optical and electrochemical data for DAPs.[a]

DAP	λ_Q [nm]	E_{ox} [V][c]	E_{red} [V][c]	ΔE [V][d]
1 Ni[b]	571	+0.80 (1 e$^-$)	−1.40 (1 e$^-$), −2.02 (1 e$^-$)	2.20
3 Ni	669	+0.74 (1 e$^-$), +0.93 (1 e$^-$)	−1.18 (1 e$^-$), −1.37 (1 e$^-$), −1.90 (1 e$^-$)	1.92
1 Cu[b]	577	+0.77 (1 e$^-$)	−1.37 (1 e$^-$), −1.95 (1 e$^-$)	2.14
3 Cu	666	+0.69 (1 e$^-$), +0.88 (1 e$^-$)	−1.21 (1 e$^-$), −1.38 (1 e$^-$), −1.96 (1 e$^-$)	1.90
6	647	+0.79 (1 e$^-$), +0.93 (1 e$^-$)	−1.26 (2 e$^-$), −1.86 (1 e$^-$), −2.05 (1 e$^-$)	2.05
7	633	+0.83 (1 e$^-$), +0.92 (1 e$^-$)	−1.36 (2 e$^-$), −1.78 (1 e$^-$), −1.91 (1 e$^-$)	2.19

[a] Measured in CH_2Cl_2 at room temperature. [b] Data from Ref. [7]. [c] Versus Fc/Fc^+. [d] $\Delta E = E_{ox,1} - E_{red,1}$.

with the order of the optical HOMO–LUMO gaps estimated from the λ_Q values.

To obtain some insight into the optical properties of the electrochemically oxidized species, we performed spectroelectrochemical measurements on **3 Ni** in CH_2Cl_2 by using Bu_4NPF_6 as the electrolyte. As shown in Figure 5, **3 Ni** displayed clear

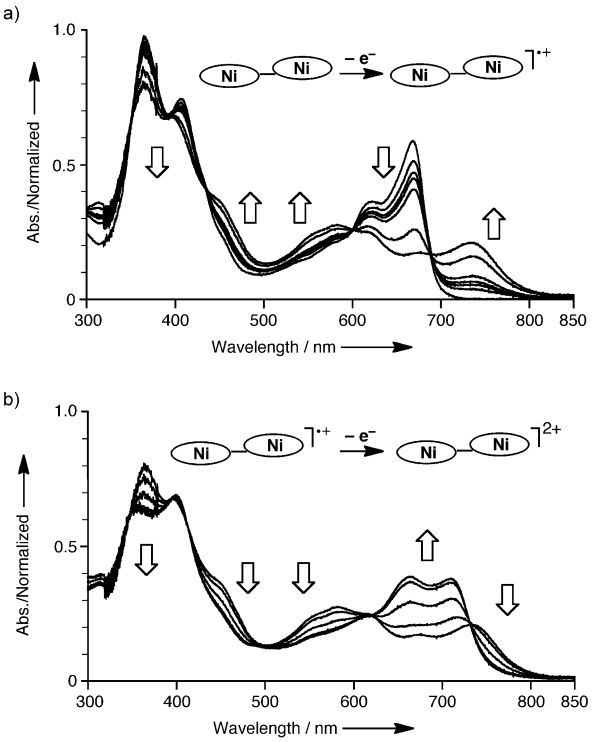

Figure 5. Spectroscopic changes observed in the electrochemical oxidation processes a) from **3 Ni** to its π-radical cation **3 Ni**$^{+\bullet}$ and b) from **3 Ni**$^{+\bullet}$ to dication **3 Ni**$^{2+}$ in CH_2Cl_2 containing Bu_4NPF_6.

spectral changes in the one-electron oxidation processes with several isosbestic points. The characteristic absorption bands of a DAP π-radical cation appeared at 700–800 nm (λ_{max} = 737 nm). In the next step, the second oxidation generated a dication, which showed characteristic absorptions at 650–750 nm (λ_{max} = 665 and 711 nm).

To investigate any exchange interaction of electron spins between the two CuDAP π systems, we also conducted electron spin resonance (ESR) measurements of **1 Cu** and **3 Cu** in toluene at 40 K (Figure 6). The monomer **1 Cu** exhibited an ESR signal (g = 2.052–2.168) with well-resolved hyperfine structures (Figure 6a). The spectral features of **1 Cu** resemble those of copper(II)–5,10,15,20-tetraphenylporphyrin (CuTPP)[14] and

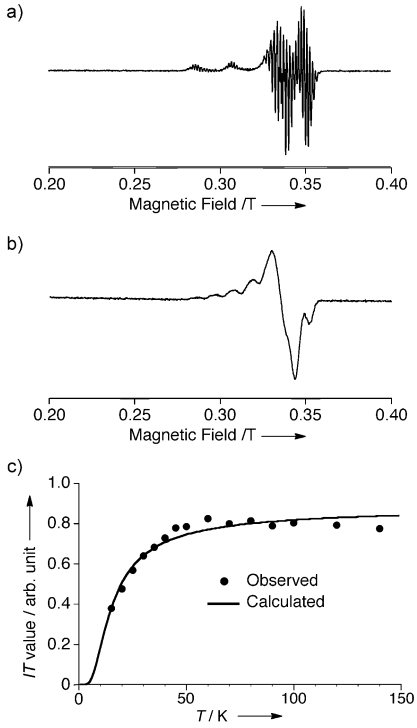

Figure 6. ESR spectra of a) **1 Cu** and b) **3 Cu** in toluene at 40 K. c) Variable-temperature ESR measurements of **3 Cu** in the range of 15 and 140 K. The solid line represents the fitting curve based on the Bleaney–Bowers equation.

–phthalocyanine (CuPc)[15] and can be simulated by taking into consideration the nuclear spins of one copper(II) and four core nitrogen atoms (Figure S6 in the Supporting Information). The spin Hamiltonian parameters of **1 Cu** are consistent with those of CuTPP and CuPc (Table S4 in the Supporting Information).[14,15] The spin densities on the *meso*-nitrogen atoms of **1 Cu** are negligible relative to those on the core atoms. The dimer **3 Cu** showed an ESR signal with the following features: 1) The hyperfine splitting for four nitrogen nuclei was merged out, and 2) the hyperfine splitting width for the copper nuclei in **3 Cu** seemed to be half that of **1 Cu** (Figure 6b). These distinguishing features could be reproduced by the spectral simulation for two magnetically coupled CuDAPs (Figure S7 in the Supporting Information). The spin Hamiltonian parameters of **3 Cu** are summarized in Table S4 in the Supporting Information.

To estimate the exchange interaction between two copper(II) spins of **3Cu**, we also examined the temperature dependence of the ESR signal intensity (*I*), which is proportional to the magnetic susceptibility. The observed *IT* values decreased sharply as the temperature dropped below 50 K (Figure 6c), which is indicative of an antiferromagnetic coupling between the two copper(II) ions. Therefore, **3Cu** appears to have a singlet ground state, and the ESR signal is likely due to a thermally populated triplet state ($S=1$). Furthermore, the observed *IT*/*T* plot of **3Cu** was fitted by the Bleaney–Bowers equation,[16] which gave an exchange coupling constant (J/k_B, in which k_B is the Boltzmann constant) of -13.8 K. It is remarkable that the $-J/k_B$ value of **3Cu** is approximately 7–15 times larger than those of Osuka's β–β-linked Cu–diporphyrin **8Cu** ($J/k_B=-0.94$ K) and triply fused Cu–diporphyrin **9** ($J/k_B=-2.06$ K).[17] The relatively large antiferromagnetic coupling of **3Cu** shows the effectiveness of the β–β direct linkage in promoting the electron-spin communication between the two DAP π systems. The complementary N···H hydrogen-bonding interaction might also contribute to the enhancement of the magnetic coupling.[18]

Conclusion

We have successfully prepared the first examples of three types of covalently linked bis-DAPs **3M**, **6**, and **7** by using palladium-catalyzed coupling reactions and investigated their optical and electrochemical properties. Both the electronic and steric effects of the *meso*-nitrogen atoms play an important role in the coplanar *trans* geometry of the directly linked bis-DAPs **3M**, which exhibits the narrowest HOMO–LUMO gaps among the series of DAP dimers examined. Such a linkage effect is unprecedented in diporphyrin chemistry and highlights the characteristics of the DAP π systems. Moreover, the ESR measurements of the directly linked bis-CuDAP **3Cu** show the relatively large long-range antiferromagnetic coupling between the paramagnetic copper(II) ions. These results confirm that the direct connection at the β positions of DAPs is highly promising for elaborating optically and magnetically coupled azaporphyrin-based materials, and further studies on covalently linked DAP derivatives are now in progress.

Experimental Section

All melting points were recorded using a Yanagimoto micro melting-point apparatus and are uncorrected. ^{1}H and ^{13}C{^{1}H} NMR spectra were recorded using a JEOL JNM-EX400 or JEOL JNM-AL300 spectrometer using CD_2Cl_2 as a solvent unless otherwise noted. Chemical shifts are reported in ppm as relative values versus tetramethylsilane. High-resolution mass spectra (HRMS) were obtained using a Thermo Fisher Scientific EXACTIVE spectrometer. UV/Vis absorption spectra were measured at room temperature using a Perkin–Elmer Lambda 900 UV/Vis-NIR spectrometer. Electrochemical measurements were performed at room temperature using a CH Instruments model 660A electrochemical workstation using a glassy carbon working electrode, a platinum wire counter electrode, and an Ag/Ag$^+$ (0.01 M $AgNO_3$, 0.1 M Bu_4NPF_6 (MeCN)) reference electrode. The potentials were calibrated with ferrocene/ferrocenium (Fc/Fc$^+$). Compounds **1Ni** and **1Cu** were prepared according to the reported procedure.[7a] Other chemicals and solvents were of reagent-grade quality and used without further purification unless otherwise noted. Thin-layer chromatography was performed using Alt. 5554 DC-Alufolien Kieselgel 60 F254 (Merck), and preparative column chromatography was performed using silica gel 60 (Nacalai Tesque). All reactions were performed under an argon atmosphere.

Synthesis and characterization of new compounds

Compound 2M: *N*-Bromosuccinimide (72 mg, 0.40 mmol) was added to a solution of **1Ni** (222 mg, 0.367 mmol) in $CHCl_3$ (100 mL), and the resulting mixture was heated under reflux conditions. After 3 h, the solvent was evaporated under reduced pressure, and the resulting solid residue was subjected to column chromatography on silica gel (CH_2Cl_2/hexane = 1:1) to give **2Ni** ($R_f=0.6$) as a purple solid (150 mg, 60%). According to a similar procedure, **2Cu** was prepared from **1Cu**. Compound **2Ni**: M.p. $>300\,^\circ$C; ^{1}H NMR (400 MHz, CD_2Cl_2): $\delta=1.79$ (s, 12H; *ortho*-Me), 2.61 (s, 6H; *para*-Me), 7.30 (s, 4H; *meta*-ArH), 8.76–8.80 (m, 3H; pyrrole-β), 8.84 (s, 1H; pyrrole-β), 9.12–9.15 (m, 2H; pyrrole-β), 9.21 ppm (d, $J=4.8$ Hz, 1H; pyrrole-β); UV/Vis (CH_2Cl_2): λ_{max} (ε) = 394 (81000), 564 nm (110000 M^{-1}cm^{-1}); HRMS (ESI): *m/z* calcd for $C_{36}H_{30}BrN_6Ni$: 683.1063; found: 683.1050 $[M+H]^+$. Compound **2Cu**: M.p. $>300\,^\circ$C; UV/Vis (CH_2Cl_2): λ_{max} (ε) = 388 (100000), 401 (110000), 582 nm (95000 M^{-1}cm^{-1}); HRMS (ESI): *m/z* calcd for $C_{36}H_{30}BrCuN_6$: 688.0992; found: 688.1006 $[M+H]^+$.

Compound 3M: A mixture of **2Ni** (33 mg, 0.048 mmol), [$PdCl_2$(dppf)] (7.1 mg, 9.7 μmol; dppf = 1,1′-bis(diphenylphosphanyl)ferrocene), potassium acetate (14 mg, 0.14 mmol), and DMF (6 mL) was stirred at 90 °C. After 5 h, toluene and water were added. The toluene layer was separated, washed with brine several times, and evaporated under reduced pressure to leave a solid residue, which was subjected to column chromatography on silica gel (hexane/CH_2Cl_2 1:1). Compound **3Ni** ($R_f=0.4$) was isolated as a green solid (26 mg, 89%). According to a similar procedure, **3Cu** was prepared from **2Cu**. Compound **3Ni**: M.p. $>300\,^\circ$C; ^{1}H NMR (400 MHz, CD_2Cl_2): $\delta=1.86$ (s, 12H; *ortho*-Me), 2.06 (s, 12H; *ortho*-Me), 2.65 (s, 6H; *para*-Me), 2.81 (s, 6H; *para*-Me), 7.34 (s, 4H; *meta*-ArH), 7.54 (s, 4H; *meta*-ArH), 8.79 (d, $J=4.8$ Hz, 2H; pyrrole-β), 8.84 (d, $J=4.4$ Hz, 2H; pyrrole-β), 8.96 (d, $J=4.8$ Hz, 2H; pyrrole-β), 8.97 (d, $J=4.8$ Hz, 2H; pyrrole-β), 9.14 (d, $J=4.4$ Hz, 2H; pyrrole-β), 9.19 (d, $J=4.8$ Hz, 2H; pyrrole-β), 11.00 ppm (s, 2H; pyrrole-β); UV/Vis (CH_2Cl_2): λ_{max} (ε) = 365 (94900), 406 (72400), 669 nm (57000 M^{-1}cm^{-1}); HRMS (ESI): *m/z* calcd for $C_{72}H_{59}N_{12}Ni_2$: 1207.3687; found: 1207.3664 $[M+H]^+$. Compound **3Cu**: M.p. $>300\,^\circ$C; UV/Vis (CH_2Cl_2): λ_{max} (ε) = 375 (89600), 410 (63000), 666 nm (61000 M^{-1}cm^{-1}); HRMS (ESI): *m/z* calcd for $C_{72}H_{59}Cu_2N_{12}$: 1217.3565; found: 1217.3572 $[M+H]^+$.

Compound 4: (Triisopropylsilyl)acetylene (35.8 mg, 0.20 mmol) was added to a mixture of **2Ni** (45 mg 0.066 mmol), CuI (3.75 mg, 0.020 mmol), [$Pd(PPh_3)_2Cl_2$] (9.2 mg, 0.013 mmol), Et_3N (0.8 mL), and THF (4.8 mL), and the resulting mixture was heated to reflux at 75 °C. After 2 h, the solvent was evaporated under reduced pressure, and the resulting solid residue was subjected to column chromatography on silica gel (hexane/EtOAc 5:1) to give **4** ($R_f=0.7$) as a purple solid (54.3 mg, 100%). M.p. $>300\,^\circ$C; ^{1}H NMR (400 MHz, CD_2Cl_2): $\delta=1.38$ (s, 21H; *i*Pr), 1.80 (s, 12H; *ortho*-Me), 2.61 (s, 6H; *para*-Me), 7.26 (s, 4H; *meta*-ArH), 8.73–8.77 (m, 4H; pyrrole-β), 9.10–9.14 ppm (m, 3H; pyrrole-β); UV/Vis (CH_2Cl_2): λ_{max} (ε) = 364 (44000), 398 (64000), 587 nm (47000 M^{-1}cm^{-1}); HRMS (ESI): *m/z* calcd for $C_{47}H_{51}N_6NiSi$: 785.3292; found: 785.3304 $[M+H]^+$.

Compound 5: Bu_4NF (THF solution, 1.0 M × 0.34 mL, 0.34 mmol) was added to a solution of **4** (54 mg, 0.069 mmol) in THF (30 mL) at room temperature. After 30 min, water and CH_2Cl_2 were added to the mixture, and the organic phase was separated, washed with brine, and evaporated under reduced pressure to give **5** as a purple solid (42 mg, 97%). ^{1}H NMR (400 MHz, CD_2Cl_2): $\delta = 1.80$ (s, 12H; *ortho*-Me), 2.61 (s, 6H; *para*-Me), 4.11 (s, 1H; ethynyl-H), 7.29 (s, 4H; *meta*-ArH), 8.77 (d, $J = 4.8$ Hz, 3×1H; pyrrole-β), 8.89 (s, 1H; pyrrole-β), 9.12 (d, $J = 4.8$ Hz, 1H; pyrrole-β), 9.13 (d, $J = 4.8$ Hz, 1H; pyrrole-β), 9.21 ppm (d, $J = 4.8$ Hz, 1H; pyrrole-β); HRMS (ESI): *m/z* calcd for $C_{38}H_{31}N_6Ni$: 629.1948; found: 629.1948 $[M+H]^+$.

Compound 6: Compound **2Ni** (43 mg, 0.063 mmol) was added to a mixture of **5** (8.0 mg, 0.013 mmol), $[Pd_2(dba)_3]$ (3.3 mg, 0.004 mmol), triphenylarsine (7.3 mg, 0.024 mmol), Et_3N (2.3 mL), and THF (14 mL), and the resulting mixture was stirred at room temperature. After 3 h, the solvent was removed under reduced pressure, and a solid residue was subjected to column chromatography on silica gel (hexane/EtOAc 5:1) to give **6** ($R_f = 0.25$) as a green solid (9.9 mg, 62% based on **5**). M.p. $> 300\,^\circ$C; ^{1}H NMR (400 MHz, CD_2Cl_2): $\delta = 1.79$ (s, 12H; *ortho*-Me), 1.90 (s, 12H; *ortho*-Me), 2.63 (s, 6H; *para*-Me), 2.66 (s, 6H; *para*-Me), 7.32 (s, 4H; *meta*-Ar–H), 7.36 (s, 4H; *meta*-Ar–H), 8.80 (d, $J = 4.4$ Hz, 2H; pyrrole-β), 8.838 (d, $J = 4.8$ Hz, 2H; pyrrole-β), 8.844 (d, $J = 4.8$ Hz, 2H; pyrrole-β), 9.157 (d, $J = 4.8$ Hz, 2H; pyrrole-β), 9.160 (d, $J = 4.8$ Hz, 2H; pyrrole-β), 9.25 (s, 2H; pyrrole-β), 9.42 ppm (d, $J = 4.8$ Hz, 2H; pyrrole-β); UV/Vis (CH_2Cl_2): λ_{max} (ε) = 366 (81 300), 405 (80 400), 647 nm (45 300 $M^{-1}cm^{-1}$); HRMS (ESI): *m/z* calcd for $C_{74}H_{59}N_{12}Ni_2$: 1233.3687; found: 1233.3675 $[M+H]^+$.

Compound 7: *N*,*N*,*N*′,*N*′-Tetramethylethylenediamine (7.8 μL, 0.069 mmol) was added to a mixture of **5** (43 mg, 0.068 mmol), CuCl (2.0 mg, 0.020 mmol), and $CHCl_3$ (18 mL) under an O_2 atmosphere, and the resulting mixture was heated at 40 °C under an O_2 atmosphere. After 24 h, the reaction mixture was subjected to column chromatography on silica gel (hexane/EtOAc = 10:1) to give **7** ($R_f = 0.30$) as a green solid (24 mg, 56%). M.p. $> 300\,^\circ$C; ^{1}H NMR (400 MHz, CD_2Cl_2): $\delta = 1.75$ (s, 12H; *ortho*-Me), 1.77 (s, 12H; *ortho*-Me), 2.54 (s, 6H; *para*-Me), 2.56 (s, 6H; *para*-Me), 7.23 (s, 4H; *meta*-Ar–H), 7.25 (s, 4H; *meta*-Ar–H), 8.68–8.74 (m, 6H; pyrrole-β), 8.95 (s, 2H; pyrrole-β), 9.045 (d, $J = 4.8$ Hz, 2H; pyrrole-β), 9.055 (d, $J = 4.80$ Hz, 2H; pyrrole-β), 9.31 ppm (d, $J = 4.8$ Hz, 2H; pyrrole-β); UV/Vis (CH_2Cl_2): λ_{max} (ε) = 367 (82 200), 407 (93 000), 633 nm (49 100 $M^{-1}cm^{-1}$); HRMS (ESI): *m/z* calcd for $C_{76}H_{59}N_{12}Ni_2$: 1255.3687; found: 1255.3695 $[M+H]^+$.

X-ray crystallographic analyses

Single crystals of **3Ni** and **3Cu** were grown from toluene/octane. All measurements were made using a Rigaku Saturn CCD area detector with graphite-monochromated $Mo_{K\alpha}$ radiation (0.71070 Å) at −130 °C. The data were corrected for Lorentz and polarization effects. The structures were solved by using direct methods (SHELXS-2013[19] or SIR-97[20]) and refined by full-matrix least-squares techniques against F^2 using SHELXL-2013.[19] The non-hydrogen atoms were refined anisotropically, and hydrogen atoms were refined using the rigid model. Compound **3Ni**: $C_{72}H_{58}N_{12}Ni_2{\cdot}2(C_7H_8)$, M_r = 1392.99; 0.40×0.30×0.20 mm, triclinic, $P\bar{1}$; $a = 12.383(2)$, $b = 14.997(3)$, $c = 20.085(4)$ Å; $\alpha = 102.184(2)$, $\beta = 96.765(2)$, $\gamma = 103.331(3)^\circ$; $V = 3493.0(11)$ Å^3; $Z = 2$; $\rho_{calcd} = 1.324$ g cm^{-3}; $\mu = 5.96$ cm^{-1}; reflections collected 28 114, independent 15 248, parameters 956; $R_w = 0.0971$ (all data), $R_1 = 0.0355$ ($I > 2\sigma(I)$); GOF = 1.093. Compound **3Cu**: $C_{72}H_{58}Cu_2N_{12}{\cdot}2(C_7H_8)$, $M_r = 1402.65$, 0.50×0.50×0.30 mm, triclinic, $P\bar{1}$; $a = 12.4306(19)$, $b = 14.882(2)$, $c = 20.257(3)$ Å; $\alpha = 101.548(2)$, $\beta = 97.5610(11)$, $\gamma = 103.8003(16)^\circ$; $V = 3501.5(9)$ Å^3; $Z = 2$; $\rho_{calcd} = 1.330$ g cm^{-3}; $\mu = 6.64$ cm^{-1}; reflections collected 28 311, independent 15 337, parameters 915; $R_w = 0.1163$ (all data), $R_1 = 0.0402$ ($I > 2\sigma(I)$); GOF = 1.074. Selected bond lengths, bond angles, torsion angles, and interatomic distances are summarized in Table S1 of the Supporting Information. Each unit cell consists of two crystallographically independent molecules, which have similar structural parameters.

CCDC-964638 (**3Ni**) and 964641 (**3Cu**) contain the supplementary crystallographic data for this paper. These data can be obtained free of charge from The Cambridge Crystallographic Data Centre via www.ccdc.cam.ac.uk/data_request/cif.

Computational details

The geometries of **3Ni-m** and **6-m** were optimized using the DFT method. The basis sets used were the 6-311G(d,p) basis set[21] for H, C, and N, and the Wachters–Hay all-electron basis set[22] supplemented with one f-function (exponent: 1.29) for Ni. The functional of DFT was the Becke three-parameter Lee–Yang–Parr (B3LYP) exchange-correlation functional.[23] We confirmed that the optimized geometries were not in saddle but in stable points. The Cartesian coordinates are summarized in Table S2 of the Supporting Information. The excitation energies and oscillator strengths listed in Table S3 of the Supporting Information were computed with the time-dependent density functional theory (TD-DFT) method, in which the solvent effect of CH_2Cl_2 was included by the polarizable continuum model (PCM) method.[24] The TD-DFT functional was the long-range corrected Becke–Lee–Yang–Parr (LC-BLYP) exchange-correlation functional.[25] All the calculations were carried out using the Gaussian 09 suite of programs.[26] Selected molecular orbitals and their energies are summarized in Figure S3 of the Supporting Information.

ESR measurements

A solution of **1Cu** or **3Cu** in toluene (1 mL) in a sealable ESR tube was degassed by repeated freeze/pump/thaw cycles and sealed under vacuum by flame. The ESR spectra were recorded using a Bruker E500 spectrometer equipped with an Oxford ESR900 He-flow-type cryostat. The temperature was controlled by using an Oxford ITC503 temperature controller. Spectral simulation was performed using the EasySpin program package.[27] The simulated spectra are in good agreement with the ones observed at 40 K (Figures S6 and S7 in the Supporting Information). The spin Hamiltonian in each spin system is indicated in Figures S6 and S7 in the Supporting Information, and the selected spin-Hamiltonian parameters are summarized in Table S4 of the Supporting Information.

The spin Hamiltonian for **1Cu** is expressed by Equation (1):

$$H = \mu_B \mathbf{S} \bullet \mathbf{g}^e \bullet \mathbf{B}_0 + \mu_N \mathbf{I}_{Cu} \bullet \mathbf{g}^n_{Cu} \bullet \mathbf{B}_0 + \mathbf{S} \bullet \mathbf{A}_{Cu} \bullet \mathbf{I}_{Cu} + \sum_i^4 [\mu_N \mathbf{I}^i_N \bullet \mathbf{g}^n_N \bullet \mathbf{B}_0 + \mathbf{S} \bullet \mathbf{A}^i_N \bullet \mathbf{I}^i_N] \quad (1)$$

in which μ_B, μ_N, **S**, **g**, **A**, $\mathbf{B}_0$, and **I** denote the Bohr magneton, the nuclear magneton, the electron-spin operator, the *g* tensor of the electron spin, the hyperfine structure tensor, the external magnetic field, and the nucleus spin operator, respectively. The spin Hamiltonian for **3Cu** is expressed by Equation (2):

$$H = (\mu_B \mathbf{S}_1 \bullet \mathbf{g}_1 \bullet \mathbf{B}_0 + \mu_N \mathbf{I}_{Cu1} \bullet \mathbf{g}_{n1} \bullet \mathbf{B}_0 + \mathbf{S}_1 \bullet \mathbf{A}_1 \bullet \mathbf{I}_{Cu1}) + (\mu_B \mathbf{S}_2 \bullet \mathbf{g}_2 \bullet \mathbf{B}_0 + \mu_N \mathbf{I}_{Cu2} \bullet \mathbf{g}_{n2} \bullet \mathbf{B}_0 + \mathbf{S}_2 \bullet \mathbf{A}_2 \bullet \mathbf{I}_{Cu2}) + \mathbf{S}_1 \bullet \mathbf{D}_{12} \bullet \mathbf{S}_2 \quad (2)$$

in which **D** stands for the fine structure tensor. The estimated spin–spin distance (9.8 Å) from the observed $|D|$ value based on the point dipole approximation is in good agreement with the determined Cu^{II}–Cu^{II} distance (9.8 Å) by X-ray diffraction.

In the case of **3 Cu**, we also examined the temperature dependence for the signal intensity *I* (Figure 4), which is proportional to the magnetic susceptibility χ, in the range of 15 and 140 K. The observed temperature dependence of *IT* values was fitted by the Bleaney–Bowers Equation (3):

$$\chi_{spin} = \frac{2Ng^2\mu_B^2}{k_B T[3 + \exp(-J/k_B T)]} \quad (3)$$

in which *N*, *g*, k_B, *T*, and *J* denote the Avogadro number, the mean value of the principal values of the *g* tensor, the Boltzmann factor, the temperature, and the exchange coupling constant, respectively. As a result, J/k_B could be estimated as −13.8 K.

Acknowledgements

This work was supported by a Grant-in-Aid (25109524 and 24109008) from the MEXT, Japan and Takahashi Foundation.

Keywords: electrochemistry · EPR spectroscopy · macrocycles · porphyrinoids · transition metals

[1] For examples, see: a) N. Aratani, A. Osuka in *Handbook of Porphyrin Science, Vol. 1* (Eds.: K. Kadish, R. M. Smith, R. Guilard), World Scientific, New Jersey, **2010**, pp. 1–132; b) Z. S. Yoon, J. Yang, H. Yoo, S. Cho, D. Kim in *Handbook of Porphyrin Science, Vol. 1* (Eds.: K. Kadish, R. M. Smith, R. Guilard), World Scientific, New Jersey, **2010**, pp. 439–505; c) M. K. Kuimova, H. A. Collins, M. Balaz, E. Dahlstedt, J. A. Levitt, N. Sergent, K. Suhling, M. Drobizhev, N. S. Makarov, A. Rebane, H. L. Anderson, D. Phillips, *Org. Biomol. Chem.* **2009**, *7*, 889; d) M. Pawlicki, H. A. Collins, R. G. Denning, H. L. Anderson, *Angew. Chem.* **2009**, *121*, 3292; *Angew. Chem. Int. Ed.* **2009**, *48*, 3244; e) M. K. Kuimova, M. Balaz, H. L. Anderson, P. R. Ogilby, *J. Am. Chem. Soc.* **2009**, *131*, 7948.

[2] For examples, see: a) V. S.-Y. Lin, S. G. DiMagno, M. J. Therien, *Science* **1994**, *264*, 1105; b) P. J. Angiolillo, V. S.-Y. Lin, J. M. Vanderkooi, M. J. Therien, *J. Am. Chem. Soc.* **1995**, *117*, 12514; c) R. Kumble, S. Palese, V. S.-Y. Lin, M. J. Therien, R. M. Hochstrasser, *J. Am. Chem. Soc.* **1998**, *120*, 11489; d) M. Drobizhev, Y. Stepanenko, Y. Dzenis, A. Karotki, A. Rebane, P. N. Taylor, H. L. Anderson, *J. Am. Chem. Soc.* **2004**, *126*, 15352; e) M. Toganoh, T. Takayama, N. Ritesh, N. Kimizuka, H. Furuta, *Chem. Lett.* **2011**, *40*, 1021.

[3] For examples, see: a) D. P. Arnold, L. J. Nitschinsk, *Tetrahedron* **1992**, *48*, 8781; b) J. J. Gosper, M. Ali, *J. Chem. Soc. Chem. Commun.* **1994**, 1707; c) B. König, H. Zieg, *Synthesis* **1998**, 171; d) P. N. Taylor, A. P. Wylie, J. Huuskonen, H. L. Anderson, *Angew. Chem.* **1998**, *110*, 1033; *Angew. Chem. Int. Ed.* **1998**, *37*, 986; e) D. P. Arnold, A. Genga, D. Manno, G. Micocci, A. Serra, A. Tepore, L. Valli, *Colloids Surf. A* **2002**, *198–200*, 897; f) L.-M. Jin, L. Chen, J.-J. Yin, J.-M. Zhou, C.-C. Guo, Q.-Y. Chen, *J. Org. Chem.* **2006**, *71*, 527; g) I. Hisaki, S. Hiroto, K. S. Kim, S. B. Noh, D. Kim, H. Shinokubo, A. Osuka, *Angew. Chem.* **2007**, *119*, 5217; *Angew. Chem. Int. Ed.* **2007**, *46*, 5125; h) C. She, S. Easwaramoorthi, P. Kim, S. Hiroto, I. Hisaki, H. Shinokubo, A. Osuka, D. Kim, J. T. Hupp, *J. Phys. Chem. A* **2010**, *114*, 3384.

[4] For examples, see: a) J. B. Paine III, D. Dolphin, M. Gouterman, *Can. J. Chem.* **1978**, *56*, 1712; b) J. Y. Becker, D. Dolphin, J. B. Paine, T. Wijesekera, *J. Electroanal. Chem.* **1984**, *164*, 335; c) Y. F. A. Chow, D. Dolphin, J. P. Paine III, D. McGarvey, R. Pottier, T. G. Truscott, *J. Photochem. Photobiol. B* **1988**, *2*, 253; d) A. Osuka, H. Shimidzu, *Angew. Chem.* **1997**, *109*, 93; *Angew. Chem. Int. Ed. Engl.* **1997**, *36*, 135; e) Y. Deng, C. K. Chang, D. G. Nocera, *Angew. Chem.* **2000**, *112*, 1108; *Angew. Chem. Int. Ed.* **2000**, *39*, 1066; f) J. T. Fletcher, M. J. Therien, *J. Am. Chem. Soc.* **2002**, *124*, 4298; g) H. Uno, Y. Kitawaki, N. Ono, *Chem. Commun.* **2002**, 116; h) H. Hata, H. Shinokubo, A. Osuka, *J. Am. Chem. Soc.* **2005**, *127*, 8264; i) G. Bringmann, S. Rüdenauer, D. C. G. Götz, T. A. M. Gulder, M. Reichert, *Org. Lett.* **2006**, *8*, 4743; j) G. Bringmann, D. C. G. Götz, T. A. M. Gulder, T. H. Gehrke, T. Bruhn, T. Kupfer, K. Radacki, H. Braunschweig, A. Heckmann, C. Lambert, *J. Am. Chem. Soc.* **2008**, *130*, 17812; k) S. Cho, M.-C. Yoon, J. M. Lim, P. Kim, N. Aratani, Y. Nakamura, T. Ikeda, A. Osuka, D. Kim, *J. Phys. Chem. B* **2009**, *113*, 10619.

[5] a) A. Osuka, A. Tsuda, *Science* **2001**, *293*, 79; b) D. Kim, A. Osuka, *J. Phys. Chem. A* **2003**, *107*, 8791; c) D. Kim, A. Osuka, *Acc. Chem. Res.* **2004**, *37*, 735; d) Y. Nakamura, N. Aratani, H. Shinokubo, A. Takagi, T. Matsumoto, Z. S. Yoon, D. Y. Kim, T. K. Ahn, D. Kim, A. Muranaka, N. Kobayashi, A. Osuka, *J. Am. Chem. Soc.* **2006**, *128*, 4119.

[6] a) N. Kobayashi in *The Porphyrin Handbook, Vol. 2* (Eds.: K. Kadish, R. M. Smith, R. Guilard), Academic Press, San Diego, **2000**, pp. 301–360; b) H. Ogata, T. Fukuda, K. Nakai, Y. Fujimura, S. Neya, P. A. Stuzhin, N. Kobayashi, *Eur. J. Org. Chem.* **2004**, 1621; c) N. Pan, Y. Bian, M. Yokoyama, R. Li, T. Fukuda, S. Neya, J. Jiang, N. Kobayashi, *Eur. J. Inorg. Chem.* **2008**, 5519.

[7] a) Y. Matano, T. Shibano, H. Nakano, H. Imahori, *Chem. Eur. J.* **2012**, *18*, 6208; b) Y. Matano, T. Shibano, H. Nakano, Y. Kimura, H. Imahori, *Inorg. Chem.* **2012**, *51*, 12879.

[8] Shinokubo and co-workers isolated a trace amount of **1 Ni** in their metal-template synthesis of azacorrole. See: M. Horie, Y. Hayashi, S. Yamaguchi, H. Shinokubo, *Chem. Eur. J.* **2012**, *18*, 5919.

[9] The DAP rings are slightly ruffled with root–mean–square deviation values (d_{RMS}) of 0.095–0.103 Å for **3 Ni** and 0.063–0.068 Å for **3 Cu**.

[10] It is well known that *meso*-nitrogen atoms of DAPs are protonated in acidic media. For example, see: P. A. Stuzhin, *J. Porphyrins Phthalocyanines* **1999**, *3*, 500; and references therein.

[11] Hydrogen bonds at the peripheral nitrogen atoms were used for the construction of a 1D chain network of N-confused porphyrins, H. Maeda, A. Osuka, H. Furuta, *Supramol. Chem.* **2003**, *15*, 447.

[12] It was reported in Ref. [4k] that a model of **8 Zn** (R^1 = H) was twisted (dihedral angle = 44.4°). For a discussion about the structure–property relationships of β–β-linked diporphyrins, see also Ref. [4i,j].

[13] 5,15-Bis(3,5-di-*tert*-butylphenyl)porphyrinatozinc(II) (λ_Q = 575 nm in toluene): A. Graja, I. Olejniczak, A. Bogucki, D. Bonifazi, F. Diedrich, *Chem. Phys.* **2004**, *300*, 227.

[14] S. P. Greiner, D. L. Rowlands, R. W. Kreilick, *J. Phys. Chem.* **1992**, *96*, 9132.

[15] C. Finazzo, C. Calle, S. Stoll, S.-V. Doorslaer, A. Schweiger, *Phys. Chem. Chem. Phys.* **2006**, *8*, 1942.

[16] R. L. Carlin, *Magnetochemistry*, Springer-Verlag, Berlin, **1986**.

[17] T. Ikeue, K. Furukawa, H. Hata, N. Aratani, H. Shinokubo, T. Kato, A. Osuka, *Angew. Chem.* **2005**, *117*, 7059; *Angew. Chem. Int. Ed.* **2005**, *44*, 6899.

[18] It has been reported that hydrogen bonds mediate magnetic coupling between two copper(II) ions: a) W. Plass, A. Pohlmann, J. Rautengarten, *Angew. Chem.* **2001**, *113*, 4333; *Angew. Chem. Int. Ed.* **2001**, *40*, 4207; b) J. Tang, J. S. Costa, A. Golobič, B. Kozlevčar, A. Robertazzi, A. V. Vargiu, P. Gamez, J. Reedijk, *Inorg. Chem.* **2009**, *48*, 5473.

[19] SHELXL-2013: G. M. Sheldrick, University of Göttingen, Göttingen, Germany.

[20] *SIR-97*: A. Altomare, M. C. Burla, M. Camalli, G. L. Cascarano, C. Giacovazzo, A. Guagliardi, A. G. G. Moliterni, G. Polidori, R. Spagna, *J. Appl. Crystallogr.* **1999**, *32*, 115.

[21] R. Krishnan, J. S. Binkley, R. Seeger, J. A. Pople, *J. Chem. Phys.* **1980**, *72*, 650.

[22] a) A. J. H. Wachters, *J. Chem. Phys.* **1970**, *52*, 1033; b) P. J. Hay, *J. Chem. Phys.* **1977**, *66*, 4377; c) K. Raghavachari, G. W. Trucks, *J. Chem. Phys.* **1989**, *91*, 1062.

[23] a) A. D. Becke, *J. Chem. Phys.* **1993**, *98*, 5648; b) C. Lee, W. Yang, R. G. Parr, *Phys. Rev. B* **1988**, *37*, 785.

[24] M. T. Cancès, B. Mennucci, J. Tomasi, *J. Chem. Phys.* **1997**, *107*, 3032.

[25] Y. Tawada, T. Tsuneda, S. Yanagisawa, T. Yanai, K. Hirao, *J. Chem. Phys.* **2004**, *120*, 8425.

[26] Gaussian 09, Revision B.01, M. J. Frisch, G. W. Trucks, H. B. Schlegel, G. E. Scuseria, M. A. Robb, J. R. Cheeseman, G. Scalmani, V. Barone, B. Mennucci, G. A. Petersson, H. Nakatsuji, M. Caricato, X. Li, H. P. Hratchian, A. F. Izmaylov, J. Bloino, G. Zheng, J. L. Sonnenberg, M. Hada, M. Ehara, K. Toyota, R. Fukuda, J. Hasegawa, M. Ishida, T. Nakajima, Y. Honda, O. Kitao, H. Nakai, T. Vreven, J. A. Montgomery, Jr., J. E. Peralta, F. Ogliaro, M. Bearpark, J. J. Heyd, E. Brothers, K. N. Kudin, V. N. Staroverov, R. Kobayashi, J. Normand, K. Raghavachari, A. Rendell, J. C. Burant, S. S. Iyengar, J. Tomasi, M. Cossi, N. Rega, J. M. Millam, M. Klene, J. E. Knox, J. B. Cross, V. Bakken, C. Adamo, J. Jaramillo, R. Gomperts, R. E. Stratmann, O. Yazyev, A. J. Austin, R. Cammi, C. Pomelli, J. W. Ochterski, R. L. Martin, K. Morokuma, V. G. Zakrzewski, G. A. Voth, P. Salvador, J. J. Dannenberg, S. Dapprich, A. D. Daniels, Ö. Farkas, J. B. Foresman, J. V. Ortiz, J. Cioslowski, D. J. Fox, Gaussian, Inc., Wallingford CT, **2009**.

[27] S. Stoll, A. Schweiger, *J. Magn. Reson.* **2006**, *178*, 42.

Received: November 26, 2013
Published online on February 12, 2014